Available online at www.sciencedirect.com

ScienceDirect

Mendeleev Commun., 2021, **31**, 319–322

Mendeleev Communications

Influence of pyridine-based ligands on photostability of $MAPbI_3$ thin films

Mayuribala Mangrulkar,*[a] Sergey Yu. Luchkin,[a] Aleksandra G. Boldyreva,[a] Pavel A. Troshin[b] and Keith J. Stevenson[a]

[a] *Skolkovo Institute of Science and Technology, 121205 Moscow, Russian Federation. E-mail: mayuribala.mangrulkar@skoltech.ru; mayuribalamangrulkar@yahoo.com*

[b] *Institute for Problems of Chemical Physics, Russian Academy of Sciences, 141432 Chernogolovka, Moscow Region, Russian Federation*

DOI: 10.1016/j.mencom.2021.05.013

The effect of pyridine-based ligands, capable of coordinating with Pb^{2+} defect sites through nitrogen atoms, on the photostability of $MAPbI_3$ thin films under solar radiation of 70–80 mW cm^{-2} at 50–60 °C in an inert atmosphere has been investigated using UV-VIS spectroscopy, X-ray diffraction analysis and atomic force microscopy. It has been found that the addition of 4,4′-bipyridine to the perovskite precursor improves the photostability of a $MAPbI_3$ thin film, withstanding illumination for 1400 h.

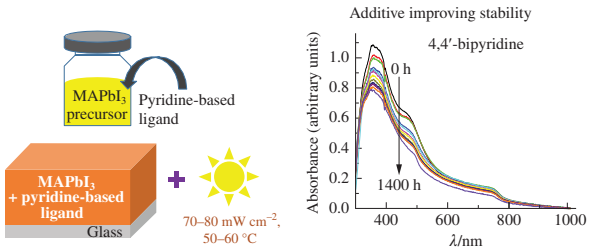

Keywords: perovskite films, perovskite solar cells, additive, pyridine-based ligand, stability, $MAPbI_3$, thin films.

Hybrid organic–inorganic lead halide perovskites have been the focus of research for the past ten years because of their outstanding optoelectronic properties, making them an attractive material for solar cell devices. The power conversion efficiency (PCE) of perovskite solar cells has now reached over 25%.[1] However, perovskite light-absorbing materials are still far from commercial use due to poor intrinsic photo- and thermal stability. Among the available light-absorbing perovskite active layers, the material $MeNH_3PbI_3$ ($MAPbI_3$) is most often studied. Unfortunately, $MAPbI_3$ tends to decompose into PbI_2 that further decomposes into the metallic lead and some other volatile species in the presence of light and heat, creating under-coordinated Pb^{2+} sites/defects due to iodine vacancy.[2–7] One way to suppress the formation of metallic lead is to passivate grain boundaries by applying a passivation layer containing the compounds with Lewis base functional groups because Pb^{2+} sites serve as defect sites that are Lewis acid in nature.[3] Another way is to use additive engineering.[8] Studies have shown that the N atom in pyridine derivatives is capable of coordinating with Pb^{2+} defect sites.[9] Usually, nitrogen-based chelating compounds are employed as passivation agents, facilitating charge carrier transport because the N atom can undergo protonation and passivate defect sites as a chelating ligand.[10–12] Hence, exploring the impact of the pyridine derivatives as additives for perovskite light-absorbing active layer is in our primary interest.

In this work, we have investigated six heterocyclic nitrogen compounds as additives for the $MAPbI_3$ active layer to achieve enhanced intrinsic photostability. These compounds were: bathophenanthroline (**1**), 4,4′-bipyridine (**2**), 4-hydroxy-1,10-phenanthroline (**3**), bathocuproine (**4**), 8-hydroxyquinoline (**5**) and 1,10-phenanthroline (**6**). The conditions for preparing thin films are described in Online Supplementary Materials. We used UV-VIS spectroscopy and X-ray diffraction (XRD) analysis to characterise the stability of $MAPbI_3$ thin films containing these additives.

The UV-VIS spectra of freshly prepared $MAPbI_3$ films [Figure 1(*a*)] illustrate that incorporating additives in the $MAPbI_3$ precursor leads to a blue shift of the absorbance edge, indicating a change in the bandgap of the perovskite layer.[13] The pristine $MAPbI_3$ film demonstrates the absorbance feature of the perovskite phase at ~750 nm. Whereas the $MAPbI_3$+(**1**) film loses the absorbance feature of perovskite, showing a small edge/bend at ~692 nm, the $MAPbI_3$+(**2**) film displays the absorbance feature at ~745 nm while retaining the perovskite phase. However, additives **3** and **4**, similar to compound **1**, destabilise the perovskite structure of the $MAPbI_3$+(**3**) and $MAPbI_3$+(**4**) films, which do not show the absorbance feature corresponding to the perovskite phase. Whereas the $MAPbI_3$+(**5**) film displays slight changes in the absorbance feature at ~730 nm, the $MAPbI_3$+(**6**) film shows a minor shift in the absorbance feature at ~736 nm due to the perovskite formation. A similar blue shift is observed for the PL emission peak upon the addition of additives **1**–**6**, accompanied by a decrease in peak intensity compared to the pristine $MAPbI_3$ film, except for compound **6** [Figure 1(*b*)].

The XRD pattern of a pristine $MAPbI_3$ film (Figure S1) displays peaks consistent with the reference cubic perovskite

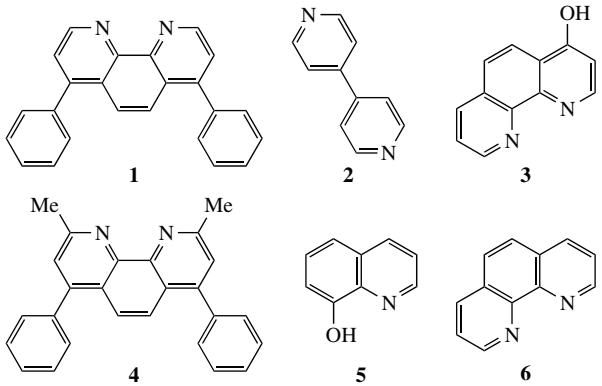

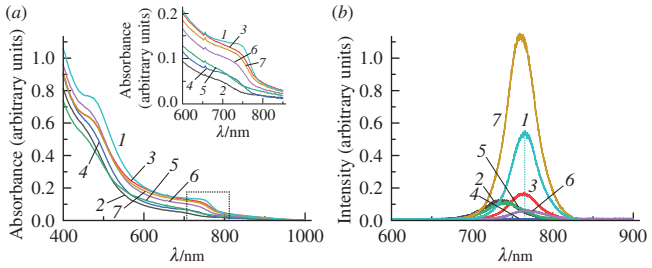

Figure 1 (*a*) UV-VIS and (*b*) PL emission spectra of (*1*) pristine $MAPbI_3$ and $MAPbI_3$ with additives (*2*) **1**, (*3*) **2**, (*4*) **3**, (*5*) **4**, (*6*) **5** and (*7*) **6**.

phase.[14] However, in the case of the $MAPbI_3$+(**1**) film, the peak corresponding to the perovskite phase is distorted, and its intensity is diminished drastically compared with pristine $MAPbI_3$, suggesting loss of crystalline nature of the film. In contrast, the $MAPbI_3$+(**2**) film displays peak splitting at 14.02 and 14.2°, which is characteristic of the perovskite structure, suggesting the phase transition in $MAPbI_3$.[15] For the $MAPbI_3$+(**3**) film, the shallower and broader peaks representing the perovskite structure are observed to be somewhat shifted than for the pristine $MAPbI_3$.[15,16] In turn, compound **4** exhibits behaviour similar to compound **1**, illustrating distortion of the perovskite structure. Films $MAPbI_3$+(**5**) and $MAPbI_3$+(**6**) demonstrate similar XRD patterns, reminiscent of $MAPbI_3$ perovskite.[15,17] Finally, a summary of UV-VIS, PL and XRD data for freshly prepared $MAPbI_3$ films with additives **1**–**6** is presented in Table 1.

Photostability tests were then carried out on all samples in a specially designed degradation chamber built into an inert atmosphere glove box. The samples were exposed to continuous light illumination with an intensity of 70–80 mW cm^{-2} at a temperature of 50–60 °C for 1400 h. Although the addition of compound **1** to the $MAPbI_3$ precursor resulted in the formation of an already distorted perovskite structure, the UV-VIS evolution of the $MAPbI_3$+(**1**) film showed fewer changes during photoaging up to 1400 h. The XRD pattern confirms the same behaviour [Figures S2(*a*),(*b*)]. For this reason, compound **1** cannot be regarded as an ideal additive for $MAPbI_3$ stabilization. In the case of compound **2**, the evolution of the UV-VIS spectrum of the $MAPbI_3$+(**2**) film shows that the absorbance feature of the perovskite structure remains noticeable after 1400 h of photoaging, indicating that the addition of compound **2** to the $MAPbI_3$ precursor improves the stability of the $MAPbI_3$ thin film [Figure S2(*c*)]. This enhanced stability can be attributed to the complex formation between PbI_2 and ligand **2** (*vide infra*).[18,19] Later, XRD measurements of the photoaged film confirmed the presence of the perovskite structure by the diffraction peak at 14.02° [Figure S2(*d*)]. However, it was found that the intensity of the corresponding peak subsequently decreased. Compounds **3** and **4** show similar behaviour to compound **1** [Figures S2(*e*)–(*h*)]. For the $MAPbI_3$+(**5**) film, the absorbance feature of the perovskite structure disappears after photoaging [Figures S2(*i*),(*j*)]. Instead, absorbance at ~500 nm is observed, indicating the decomposition of perovskite and the formation of PbI_2. The XRD patterns of the photoaged $MAPbI_3$+(**5**) film later confirmed the formation of PbI_2 and Pb from the diffraction peaks at 12.6 and 31.1°, respectively.[20] Likewise, the $MAPbI_3$+(**6**) film also shows the formation of Pb and suggests that the addition of compound **6** also destabilises $MAPbI_3$ [Figures S2(*k*),(*l*)]. In contrast, the pristine $MAPbI_3$ decomposes into PbI_2 and Pb as expected[2] [Figures S2(*m*),(*n*)].

To better visualise the dynamics of photoaging, we normalised UV-VIS spectra at a characteristic wavelength of 700 nm [Figure 2(*a*)]. We chose this wavelength because 700–800 nm is the region where the absorbance feature of $MAPbI_3$ usually appears.[21] Figure 2(*b*) presents the phase composition of the films subjected to 1400 h of photoaging based on the qualitative analysis of XRD data. In the UV-VIS graph, compound **1** demonstrates the highest normalised absorbance. As mentioned above, compound **1** results in a distorted absorbance edge at ~692 nm, eliminating the absorbance feature of $MAPbI_3$. Therefore, we cannot regard compound **1** as a stabilising agent. Next, the second-highest normalised absorbance is demonstrated by compound **2**, which enhances the intrinsic photostability of the $MAPbI_3$ thin film [Figure 2(*a*)]. Also, XRD analysis of phase composition shows favourable results for $MAPbI_3$+(**2**) [Figure 2(*b*)].

Finally, we examined the samples with atomic force microscopy (AFM). Pristine $MAPbI_3$ has a heterogeneous surface with more or less significant clusters [Figure 3(*a*)]. In contrast, AFM images revealed that the $MAPbI_3$+(**2**) film exhibits a uniform, dense, compact, fine-grained structure [Figure 3(*b*)]. Despite the presence of morphological differences between the pristine $MAPbI_3$ and $MAPbI_3$+(**2**) films, the root-mean-square (RMS) roughness is similar. Pinholes appear on the pristine $MAPbI_3$ film after photoaging, indicating photodegradation of the perovskite structure [Figure 3(*c*)]. In contrast, $MAPbI_3$+(**2**) shows the growth of needle-like structure, which indicates the formation of a new complex, resulting in enhanced photostability of the thin film [Figure 3(*d*)]. For comparison, the film morphology for additives **1**–**6** is shown in Figure S3.

Further, we compared the PL spectra of the pristine and $MAPbI_3$+(**2**) samples (Figure S4). Freshly prepared pristine $MAPbI_3$ exhibits a higher PL peak intensity than $MAPbI_3$+(**2**), suggesting that compound **2** can lead to more non-radiative losses responsible for a decrease in open-circuit voltage and fill factor[16]. However, after photoaging, the PL emission peak of the pristine $MAPbI_3$ disappears, while the intensity of $MAPbI_3$+(**2**) emission peak becomes higher than for the fresh sample. Besides, the PL emission peak of $MAPbI_3$+(**2**) demonstrates an additional

Table 1 Overview of UV-VIS, PL and XRD data for freshly prepared $MAPbI_3$ films with additives **1**–**6**.

Additive in $MAPbI_3$	Position of UV-VIS absorbance edge/nm	PL peak position/nm	XRD peak positions/deg
No	750	767	14.1, 28.4 and 31.9
1	692[a]	734	[a]
2	745	764	14.02, 14.2, 28.4 and 31.9
3	710	723	13.9, 14.3, 28.6 and 32.0
4	690[a]	746	[a]
5	730	766	14.02, 14.2, 28.4 and 31.8
6	736	758	14.02, 14.2, 28.4 and 31.8

[a] Diminished signal intensity.

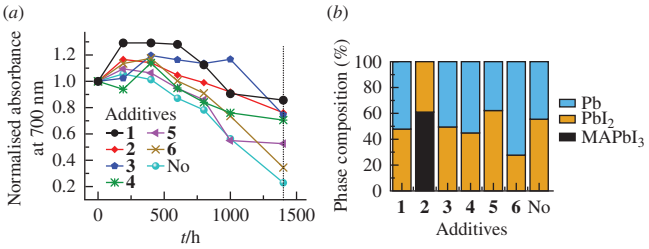

Figure 2 Influence of compounds **1**–**6** on the photostability of $MAPbI_3$ thin films. (*a*) Evolution of the normalised absorbance of photoaged films with and without additives. (*b*) Phase composition of photoaged films with and without additives after 1400 h. Conditions for photoaging: light intensity of 70–80 mW cm^{-2}, temperature of 50–60 °C. The amount of a phase was estimated by the XRD peak intensity ratio I_{1400}/I_0.

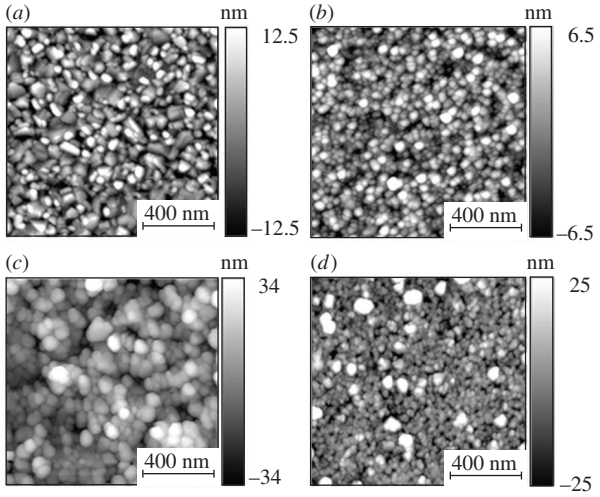

Figure 3 AFM images of the freshly prepared (*a*) pristine $MAPbI_3$ and (*b*) $MAPbI_3$+(**2**) films as well as the photoaged (*c*) pristine $MAPbI_3$ and (*d*) $MAPbI_3$+(**2**) films. The RMS roughness of the films is (*a*) 5.5, (*b*) 5.4, (*c*) 16 and (*d*) 13 nm.

blue shift during photoaging, which can be explained by complex formation upon the addition of compound **2** to $MAPbI_3$.[22]

Using FTIR spectroscopy, we investigated the formation of complexes (Figure 4). The results showed that the Pb^{2+} sites in $MAPbI_3$ act as Lewis acids, while the electron-deficient nitrogen-containing heterocyclic compounds behave as Lewis bases, and their coordination leads to the formation of the Lewis acid–base adduct.[23,24] Hence, the complexation between PbI_2 and compound **2** should be expected. The FTIR spectra of pristine $MAPbI_3$ show peaks corresponding to the perovskite structure at 1468 and 1580 (N–H bending), 2926 (C–H bending), as well as 3136 and 3175 cm^{-1} (N–H stretching), which is consistent with the known data.[14] In the FTIR spectrum of $MAPbI_3$+(**2**), the peaks of N–H bending turn out to be shifted to 1466 and 1573 cm^{-1}. Also, many minor peaks appear at ~1573 cm^{-1}, indicating the formation of a new complex between PbI_2 and ligand **2**.[22,25] Besides, a minor peak of PbI_2 appears at ~2965 cm^{-1} along with the peak of C–H stretching at ~2925 cm^{-1}. The peaks corresponding to the N–H stretching are also shifted to 3130 and 3178 cm^{-1} due to the PbI_2–(**2**) complex formation. The peaks corresponding to complex formation are attributed to a minor ring stretching vibrations at 1436, 1490 and 1573 cm^{-1}.[22] The peak at 1557 cm^{-1} is assigned to ligand **2**[22] (Figure S5). This complex formation also explains the decrease and shift of the absorbance edge around 500 nm attributed to PbI_2[19] (Figure S7) and ultimately results in improved stability of the $MAPbI_3$+(**2**) thin film (Figure S6).

Since compound **2** improves the intrinsic photochemical stability of $MAPbI_3$, we further tested this additive in solar cell devices with n-i-p configuration [Figure S8(*a*)]. Concentration

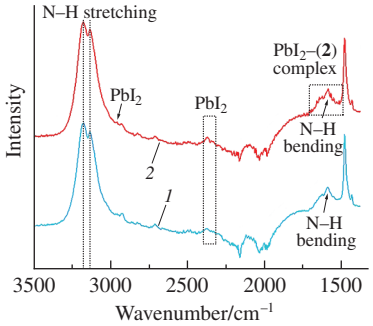

Figure 4 FTIR spectra of the freshly prepared (*1*) pristine $MAPbI_3$ and (*2*) $MAPbI_3$+(**2**) thin films.

of ligand **2** varied as 0.0 (pristine), 0.5, 1, 2.5, 5 and 7.5 wt%. The distribution of *J*–*V* parameters (including both forward and reverse scans) are shown in Figure S8(*b*). Unfortunately, the addition of ligand **2** slightly lowers the PCE (15.4%) as compared to the pristine device (16.9%). The best and average device parameters for different concentrations of ligand **2** in $MAPbI_3$ are given in Table S1. A slight decrease in PCE is due to the lower V_{oc} and fill factor, which can be attributed to higher non-radiative losses.[13] However, using excess PbI_2[26] or facilitating charge transport by additional layers can be further applied in combination with ligand **2** to achieve a higher PCE and is the subject of further research and optimisation. In addition, the hysteresis factor was calculated for the optimum concentration (2.5%) and compared with the pristine one, presented in Figure S9 and Table S2. The hysteresis factor was calculated using the formula reported elsewhere:[27]

$$\text{Hysteresis factor} = \frac{\text{PCE (reverse)} - \text{PCE (forward)}}{\text{PCE (reverse)}}. \quad (1)$$

Based on the *J*–*V* parameters and hysteresis factor, it can be seen that the performance of $MAPbI_3$+(**2**) is comparable to that of the pristine perovskite. Hence, $MAPbI_3$+(**2**) can be used in photovoltaic applications.

In summary, we have investigated the influence of nitrogen-containing heterocyclic compounds on the photostability of the $MAPbI_3$ thin film. UV-VIS and XRD results demonstrated that the addition of 4,4′-bipyridine (**2**) enhances the intrinsic photostability of the $MAPbI_3$ film. Further, PL measurements and AFM topography suggested complex formation upon the addition of ligand **2**. Finally, the characteristic FTIR peak confirmed the complexation with 4,4′-bipyridine, which is perceived as the reason for increasing photostability of the $MAPbI_3$ film.

The support from the Ministry of Science and Higher Education of the Russian Federation (project no. 0089-2019-0010/AAAA-A19-119071190044-3) at IPCP RAS (Institute for Problems of Chemical Physics of the Russian Academy of Sciences) is acknowledged.

Online Supplementary Materials

Supplementary data associated with this article can be found in the online version at doi: 10.1016/j.mencom.2021.05.013.

References

1 Best Research-Cell Efficiency Chart, the National Renewable Energy Laboratory, Golden, CO, December 12, 2020, https://www.nrel.gov/pv/cell-efficiency.html.
2 E. J. Juarez-Perez, L. K. Ono, M. Maeda, Y. Jiang, Z. Hawash and Y. Qi, *J. Mater. Chem. A*, 2018, **6**, 9604.
3 L. K. Ono, S. Liu and Y. Qi, *Angew. Chem., Int. Ed.*, 2020, **59**, 6676.
4 A. Latini, G. Gigli and A. Ciccioli, *Sustainable Energy Fuels*, 2017, **1**, 1351.
5 A. F. Akbulatov, L. A. Frolova, N. N. Dremova, I. Zhidkov, V. M. Martynenko, S. A. Tsarev, S. Yu. Luchkin, E. Z. Kurmaev, S. M. Aldoshin, K. J. Stevenson and P. A. Troshin, *J. Phys. Chem. Lett.*, 2020, **11**, 333.
6 A. F. Akbulatov, S. Yu. Luchkin, L. A. Frolova, N. N. Dremova, K. L. Gerasimov, I. S. Zhidkov, D. V. Anokhin, E. Z. Kurmaev, K. J. Stevenson and P. A. Troshin, *J. Phys. Chem. Lett.*, 2017, **8**, 1211.
7 B. Brunetti, C. Cavallo, A. Ciccioli, G. Gigli and A. Latini, *Sci. Rep.*, 2017, **7**, 46867.
8 F. Zhang and K. Zhu, *Adv. Energy Mater.*, 2020, **10**, 1902579.
9 L. Zhang and J. M. Cole, *ACS Appl. Mater. Interfaces*, 2015, **7**, 3427.
10 M.-C. Hsiao, P.-C. Chien, L.-S. Jhuang and F.-C. Chen, *Phys. Chem. Chem. Phys.*, 2019, **21**, 7867.
11 G. Accorsi, A. Listorti, K. Yoosaf and N. Armaroli, *Chem. Soc. Rev.*, 2009, **38**, 1690.

12 E. I. Marchenko, S. A. Fateev, A. A. Petrov, E. A. Goodilin and A. B. Tarasov, *Mendeleev Commun.*, 2020, **30**, 279.
13 P.-P. Cheng, Y.-W. Zhang, J.-M. Liang, W.-Y. Tan, X. Chen, Y. Liu and Y. Min, *Sol. Energy*, 2019, **190**, 264.
14 X. Yu, H. Yan and Q. Peng, *J. Phys. Chem. A*, 2017, **121**, 6755.
15 T. Oku, in *Solar Cells – New Approaches and Reviews*, ed. L. A. Kosyachenko, InTech, Rijeka, Croatia, 2015, pp. 77–101.
16 J. Chen, S.-G. Kim, X. Ren, H. S. Jung and N.-G. Park, *J. Mater. Chem. A*, 2019, **7**, 4977.
17 Y. Yue, N. T. Salim, Y. Wu, X. Yang, A. Islam, W. Chen, J. Liu, E. Bi, F. Xie, M. Cai and L. Han, *Adv. Mater.*, 2016, **28**, 10738.
18 S. M. Jain, Z. Qiu, L. Häggman, M. Mirmohades, M. B. Johansson, T. Edvinsson and G. Boschloo, *Energy Environ. Sci.*, 2016, **9**, 3770.
19 H. Zhang, J. Cheng, D. Li, F. Lin, J. Mao, C. Liang, A. K.-Y. Jen, M. Grätzel and W. C. H. Choy, *Adv. Mater.*, 2017, **29**, 1604695.
20 M. Wang, C. Shi, J. Zhang, N. Wu and C. Ying, *J. Solid State Chem.*, 2015, **231**, 20.
21 T. Wang, *PhD Thesis*, University of Amsterdam, 2019.
22 N. Preda, L. Mihut, M. Baibarac, I. Baltog, M. Husanu, C. Bucur and T. Velula, *Rom. J. Phys.*, 2009, **54**, 667.
23 A. Morsali and X.-M. Chen, *J. Coord. Chem.*, 2004, **57**, 1233.
24 H. Miyamae, H. Toriyama, T. Abe, G. Hihara and M. Nagata, *Acta Crystallogr., Sect. C: Cryst. Struct. Commun.*, 1984, **40**, 1559.
25 I. Wharf, T. Gramstad, R. Makhija and M. Onyszchuk, *Can. J. Chem.*, 1976, **54**, 3430.
26 C. Roldán-Carmona, P. Gratia, I. Zimmermann, G. Grancini, P. Gao, M. Graetzel and M. K. Nazeeruddin, *Energy Environ. Sci.*, 2015, **8**, 3550.
27 S. N. Habisreutinger, N. K. Noel and H. J. Snaith, *ACS Energy Lett.*, 2018, **3**, 2472.

Received: 3rd February 2021; Com. 21/6439